DOI: 10.2352/ISSN.2470-1173.2016.19.COIMG-157

Reducing restoration artifacts in 3D computational microscopy using wavefront encoding

Nurmohammed Patwary and Chrysanthe Preza
Department of Electrical and Computer Engineering, University of Memphis, TN 38152, USA

Abstract

Depth-induced spherical aberration in three-dimensional (3D) microscopy causes the 3D system response to vary with imaging depth within the sample. In order to overcome restoration artifacts, depth-variant restoration algorithms have been developed, which are computationally intensive. In this paper, we present an approach based on wavefront encoding that enables restoration of images from a thick object using a space-invariant algorithm. Experimental validation of an imaging system in which the pupil is modified by a phase mask, thereby rendering the point spread function less sensitive to imaging depth is demonstrated. Simulated results using a 63X/1.4 NA oil immersion microscope objective lens show that it is possible to restore images of a 30 µm thick sample using a SI approach with reduced artifacts compared to restorations of images from the conventional system. Our results are validated using experimental images.

Introduction

Wide field fluorescence microscopy (WFM) is preferable for live-cell imaging because it is non-invasive and provides fast data acquisition. In WFM, three-dimensional (3D) imaging is achieved by acquiring 2D images at different focal planes and then processed using knowledge of the microscope's point spread function (PSF). During the image formation process, refractive index difference between the microscope objective lens' immersion medium and the specimen's mounting medium results in spherical aberration (SA), which increases with depth. This depth-dependent SA makes imaging system depth-variant (DV) and thus DV image restoration algorithms [1, 2] are needed to reconstruct the images without artifacts. DV algorithms take a long time to execute and require large amounts of memory. In this paper, we present an approach based on wavefront encoding that allows the use of space-invariant (SI) algorithms instead.

The method of modifying the pupil of an imaging system, known as wavefront encoding (WFE), was initially used in extended depth-of-field microscopy [3]. The use of WFE to reduce depth-variability in computational optical sectioning microscopy (COSM) was initially proposed based on a selected cubic phase mask design, which rendered the point spread function (PSF) less sensitive to imaging depth [4]. Later, the squared cubic (SQUBIC) phase mask [5], designed to reduce the effect of depth induced SA in microscopy, was also applied to COSM [6, 7]. The WFE PSF based on the SQUBIC phase mask varies slowly with increasing depth compared to the PSFs of the conventional imaging system, making the use of SI restoration algorithms applicable over a wide range of imaging depth [6]. Thus, a SQUIBIC WFE microscope system has the potential to reduce the requirement of computational resources (i.e. execution time and memory) in the image restoration process without sacrificing image quality, which is a vital requirement for the 3D live-cell imaging. In this paper, experimental validation of the use of SQUBIC-WFE in COSM is presented. Preliminary results of this study appeared in earlier publications [6-8]

In this paper, we investigate the performance of the SQUBIC phase mask in reducing the effect of depth induced SA in WFM. The SQUBIC phase mask values vary with one of the design parameters *(A)* [7], and the mask's theoretical performance (i.e. capability of reducing depth sensitivity) increases with the increase of the value of *A*. The effect of the design parameter *A* on the system PSF is quantified in this study. The performance of the SQUBIC phase mask in quantitative imaging of thick samples through 3D restoration is studied both in simulation and experiment.

Theory

PSF of the WFE system

In optical sectioning microscopy, a 3D volume is acquired by refocusing through the sample along the axis of light propagation (Z-axis) and capturing 2D images at multiple imaging depths. In WFE, the phase of the specimen-emitted light wavefront is modified at the back focal plane of the objective lens [9]. To calculate WFE-PSFs from conventional PSFs, the generalized pupil function is calculated by adding the SQUBIC phase mask function $\phi(f_x, f_y)$ to the conventional pupil phase of the Fourier transform of each plane of the conventional PSF. This process is described by the following equation [4]:

$$h_{z_i,z_o}(x,y) = \left| F^{-1}\left\{ H(f_x,f_y) e^{j(2\pi/\lambda)W(f_x,f_y;z_o)} e^{j\varphi(f_x,f_y)} \right\} \right|^2, \qquad (1)$$

where $F^{-1}\{\bullet\}$ is the 2-D inverse Fourier transform; $H(f_x,f_y)$ is the optical transfer function (OTF) of the conventional imaging system; λ is the emission wavelength; and $W(f_x,f_y;z_i,z_o)$ is the optical path length due to defocus and SA. The 3D WFE PSF for a point-source located at depth z_o in the sample, formed by stacking all the 2D axial planes computed with Eq. (1), is defined by:

$$h(x,y,z_i;z_o) = h_{z_i,z_o}(x,y). \qquad (2)$$

The SQUBIC phase mask

The values of the SQUBIC phase mask used in this study were computed using the following equation [6]:

$$\varphi(\rho,\alpha) = 2\pi A \left[\frac{\sqrt{1-\rho^2 \sin^2(\alpha)} - 1}{1-\cos(\alpha)} + \frac{1}{2} \right]^3, \qquad (3)$$

©2016 Society for Imaging Science and Technology
DOI: 10.2352/ISSN.2470-1173.2016.19.COIMG-157

where $\rho=\sqrt{f_x^2+f_y^2}$ and $\alpha=\sin^{-1}(NA/n)$ with n the refractive index (RI) of the lens' immersion medium, and NA is the numerical aperture of the objective lens. The design parameter A is a measure of the strength of the mask and determines its ability to reduce the effect of depth induced SA. The performance of the SQUBIC phase mask is improved when the value of A is increased [7].

Forward image formation model and restoration

Using 3D DV-PSFs defined at each depth (Eq. 2), the intensity in the forward image of an object can be defined by the superposition integral [4]:

$$g(\mathbf{x_i})=\iiint_O h(x_i-x_o,y_i-y_o,z_i;z_o)\,f(\mathbf{x}_o)\,d\mathbf{x}_o, \tag{4}$$

where $\mathbf{x_i}=(x_i,y_i,z_i)$ is a 3D point in the image space; $\mathbf{x}_o=(x_o,y_o,z_o)$ is a 3D point in the object space O; $f(\mathbf{x_o})$ is the object intensity. Eq. 4 has successfully approximated by the strata-based forward imaging model, which uses only a finite number of DV-PSFs over the entire thickness of the sample [1], and the PCA based depth-variant imaging model [2, 10]. In this study, we used the strata-based approximation model to compute the WFM forward image of the test object.

Both the simulated forward image and the experimentally acquired images were restored using the space-invariant expectation maximization (SIEM) algorithm [11], which assumes the imaging system does not change along the depth and uses a single PSF to reconstruct the whole volume. In the SIEM algorithm, the image intensity at the (k+1)-th iteration is estimated by updating the current estimate $s^k(x,y,z)$, by a back projection to the object space of the measured image $g(x,y,z)$, divided by the model prediction at the k-th iteration $g^k(x,y,z)$, as in following iteration step:

$$s^{k+1}(x,y,z)=\frac{s^k(x,y,z)}{H_{z_o}}\cdot\left[h(-x,-y,-z;z_o)\otimes\frac{g(x,y,z)}{g^k(x,y,z)}\right], \tag{5}$$

where H_{z_o} is the sum of intensity in the 3D PSF, $h(x,y,z;z_o)$. As the inverse imaging problem is ill-posed, the solution was stabilized using Tikhonov-Miller regularization with the Good's roughness penalty [12].

Methods

Experimental setup

The WFE system was implemented in a Zeiss Imager.Z1 microscope, which was modified to have two imaging paths: (i) a top imaging path for conventional imaging, and (ii) a side imaging path for WFE imaging. We implemented the WFE in the side imaging path through a 4F imaging system using a liquid crystal reflective spatial light modulator (LC-SLM), which was placed at the Fourier plane of the 4F configuration, thereby altering the phase of the incident wavefront by a desired function [13]. A schematic of the WFE implementation is depicted in Figure 1a where it is seen that the SLM is placed at 20° angle with the incoming wavefront. This oblique angle causes the pupil of the image plane (which is a conjugate plane to the Fourier plane of the 4F system) to change its shape from circular to elliptical (Figure 1b). The ratio of the major and minor axes of the ellipse is the cosine of the angle between the normal of the SLM's reflective surface and the incoming wavefront (i.e. 20° in this setup). Details of the WFE implementation are reported in Ref. [13]. The top view of the experimental configuration is shown in Figure 1(c).

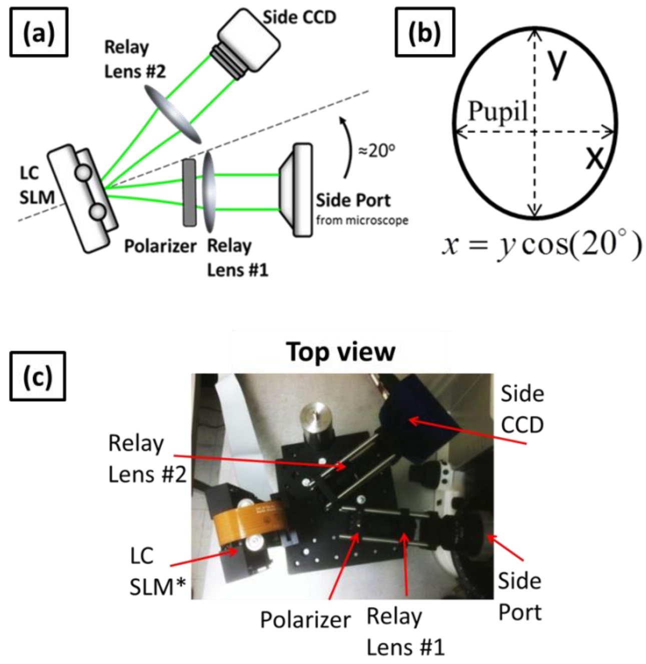

Figure 1: Experimental setup for wavefront encoding implemented on a commercial upright microscope. (a) Schematic of the WFE setup, which uses a liquid crustal spatial light modulator (LC-SLM). (b) The elliptical pupil due to the oblique illumination. (c) Top view of the experimental configuration.

Sample preparation

The test sample used in this study was prepared using 6-µm in diameter fluorescence micro spheres with two fluorescent markers: 1) a blue marker that labels it throughout; and 2) a green marker that labels only a 1-µm thick outer shell (Invitrogen, Molecular Probes®, FocalCheck™ microspheres, 6 µm fluorescent green ring stain/blue throughout). The micro spheres were dried on the microscope slide and embedded in ProLong® diamond (RI = 1.47). Some 170-nm in diameter spheres were also dried on the cover slip to use as reference of zero depth (interface between the cover slip and the sample medium). The lower surface of the cover glass was also scratched using a diamond pen to use as a marker of the interface between the cover slip and the sample medium.

Image acquisition

Images of the test sample were captured using the modified Zeiss Imager.Z1, with a 63X/1.4 NA oil (RI = 1.518) immersion objective lens and a green fluorescent filter set with excitation wavelength 450-460 nm, and emission wavelength 515-565 nm, thus, the light emitted from the object appeared as a spherical shell. The sample was illuminated using a mercury-arc source. Conventional images were captured using the top imaging path and sequentially SQUBIC images were captured from the side imaging

DOI: 10.2352/ISSN.2470-1173.2016.19.COIMG-157

path. A SQUBIC phase mask with design parameter A = -20 was projected onto the SLM to implement the WFE system. Our phase mask implementation with the SLM presents challenges for |A| > 20 resulting in WFE-PSFs that deviate from simulation [13].

Images of three different micro spheres, located at depths d_0 µm, d_0+12 µm and d_0+27 µm, were captured. To calculate the d_0 depth, both the 170 nm fluorescent beads, and the scratch on the cover slip (imaged using the Differential Interference Contrast configuration) were used as reference, and in each case, we found the cover glass and embedding medium interface with an accuracy of ±2 µm.

Computation of conventional and WFE PSFs

PSFs were generated on a 256 × 256 × 512 grid with a voxel dimension of 0.1 µm × 0.1 µm × 0.1 µm for a 63X/1.4 NA oil immersion objective lens with a 515 nm emission wavelength and RI = 1.47 as the specimen embedding medium. The PSFs were generated in MATLAB using the Gibson-Lanni optical path distance (OPD) model [14] and the vectorial field approximation [15]. As the SLM was illuminated at an oblique angle, the WFE-PSFs were calculated with an elliptical SQUBIC-modified pupil, $H(f_x, f_y)$, as described in the experimental method section (Figure 1b). The 3D WFE-PSFs used in this study were computed using a SQUBIC phase mask with design parameter A equal to -20 and -50.

Simulated image formation and restoration

Simulated image of a 6 µm in diameter spherical shell with a shell thickness equal to 1 µm was generated (to mimic the experiment). Three images were simulated using DV-PSFs computed at depths at 0 µm, 12 µm and 27 µm, respectively for a conventional and a WFE system for A equal to -20 and -50. The images were simulated using the *CosmTools* module of the open source software package COSMOS [16] which implements Eq. (4) using the strata approximation approach. The images were simulated on a 512 × 512 × 700 grid where each voxel was mapped to a physical dimension of 0.1 µm^3, using 6 strata with a 1µm separation (i.e., 7 DV-PSFs).

Image restoration

Both the simulated and experimental images were restored using the regularized SIEM algorithm implemented in COSMOS [16]. The simulated images were restored without any regularization penalty (as they are noise free), whereas for the restoration of the experimental images a regularization parameter equal to 0.005 was used. Restoration results shown here were obtained after 1000 iterations of the SIEM algorithm.

Performance evaluation metrics

The PSFs of the conventional and the SQUBIC-WFE system were compared using the structural similarity index (SSIM) [17] computed between the PSF at a 0-µm depth and PSFs at other depths. The SSIM quantifies the differences between two images in terms of: (i) image illumination; (ii) contrast; and (iii) structure, which are calculated from the image means, variances, and correlation coefficient between the two images, respectively. As with the change of depths, the PSFs changes in all attributes mentioned above (i.e. illumination, contrast, and structure), the SSIM can be considered as a good comparison metric to quantify the change in PSFs at different depths. The SSIM between two 3D volumetric images X, and Y is defined by the following equation:

$$\Gamma(X,Y) = \frac{(2\mu_X\mu_Y + c_1)(2\sigma_{XY} + c_2)}{(\mu_X^2 + \mu_Y^2 + c_1)(\sigma_X^2 + \sigma_Y^2 + c_2)}, \tag{6}$$

where μ_X, μ_Y and σ_X, σ_Y are the mean and variance of the corresponding images; σ_{XY} is the covariance between the images; and c_1 and c_2 are two constants, which restrict the value of SSIM from growing to infinity. In general, the value of SSIM ranges from -1 to +1, however, in the case of fluorescence microcopy (where only positive intensities are captured), the minimum and maximum values of SSIM are 0 and 1, respectively, which refer to 0% or 100% match between the intensity distributions of two images.

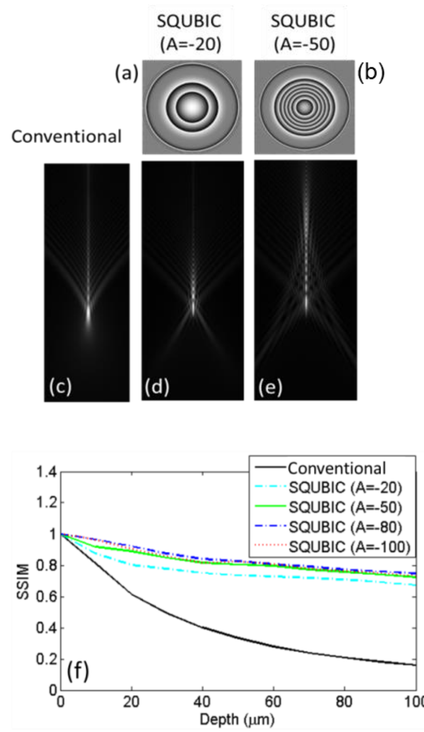

Figure 2: SQUBIC-WFE system demonstrates depth-invariance compared to conventional system. Comparison between conventional and SQUBIC PSFs: (a-b) Wrapped phase for SQUBIC masks with A = -20 and A = -50, respectively; (c-e) XZ sectional images of the conventional (c), SQUBIC A = -20 (d), and SQUBIC A = -50 (e) PSFs, respectively. (f) Change of the SSIM with respect to depth for different imaging conditions.

The test object used in this study is a 6 µm in diameter spherical shell having shell thickness equal to one with equal intensity throughout the volume. To quantify how the structure of the test object is restored in the final image, the correlation coefficient between two images was used. The correlation coefficient (ψ) was computed using the following equation:

$$\psi = \frac{\sigma_{XY} + C_3}{\sigma_X\sigma_Y + C_3}, \tag{7}$$

©2016 Society for Imaging Science and Technology
DOI: 10.2352/ISSN.2470-1173.2016.19.COIMG-157

where C_3 is a constant. Both the SSIM and correlation coefficients were calculated on a region of interest (ROI) of the images, and the ROI was normalized from zero to one to reduce bias from the background of the images. As these metrics are dependent on image registration, experimental images were registered properly to match the ROI.

Results

Depth stability of the SQUBIC WFE PSFs

A comparative study between conventional and SQUBIC WFE imaging is shown in Figure 2 where XZ sectional view images of the conventional and SQUBIC WFE PSFs at depth 50 µm are shown. Figure 2 (a) and (b) show the SQUBIC phase masks for the design parameter A = -20, and A = -50. The conventional and the SQUBIC PSFs are shown in Figure 2(c), (d), and (e), respectively. The change of the PSFs at different depths computed in terms of the SSIM between the PSF at 0 µm depth and PSFs at other depths for various values of A is plotted as a function of depth in Figure 2(f), where it is seen that the conventional PSFs vary rapidly with the increase of depth compared to the SQUBIC WFE PSFs. Furthermore, stability of the SQUBIC WFE PSFs increases with the increase of the value of the design parameter A, as predicted by the analytical studies [7].

Imaging performacne in simulations

Figure 3 shows image restoration improvements in simulation achieved with the SQUBIC-WFE system compared to the conventional system where SIEM restored images of beads at depths 3 µm, 12 µm and 27 µm, using a PSF computed at either depth 3 µm or 27 µm below the cover slip are compared.

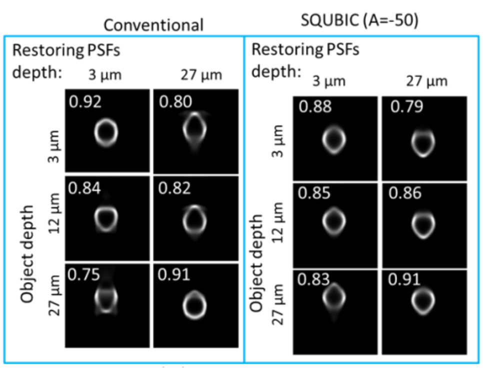

Figure 3: Performance comparison between the conventional and SQUBIC system in restoring beads at different depths in simulation. XZ sectional view of the restored images of three 6 µm in diameter spherical shells centered at depths 3 µm, 12 µm, and 27 µm in the case of conventional (left) and SQUBIC (A=-50) simulated images (right). The correlation coefficient value reported inside each image is computed between the true numerical object and the restored image. Images are displayed on their own intensity scale to show details in each case. Lens: 63X/1.4 NA oil immersion objective lens, RI of the specimen embedding medium = 1.47, emission wavelength is 515 nm.

The correlation coefficients shown on the images are computed between the XZ sectional view images of the true object and the restored images quantify that in the SQUBIC case, the restoration is less dependent on the choice of the PSF depth. The standard deviation between the correlation coefficients in the case of the conventional and SQUBIC restorations are 0.0654, and 0.0413, respectively. The higher correlation values with a lower standard deviation between them quantify the improved restoration accuracy and reduced depth sensitivity achieved in the SQUBIC WFE system.

Performance of the SQUBIC WFE system in experiment

The comparison between the experimental and simulated forward image in the case of SQUBIC (A = -20) WFE system is shown in Figure 4 where the XZ sectional view of an experimentally acquired image from depth 12 µm, and three simulated images at depths depth 0 µm, 12 µm and 27 µm are shown. From a visual inspection, it is seen that the simulated images resemble the experiment and simulated images at different depths have similar intensity distribution. The correlation coefficient computed between the experimental image and the simulated images is 0.98 in all three cases, which also suggests the reduced depth invariance of the SQUBIC WFE imaging system.

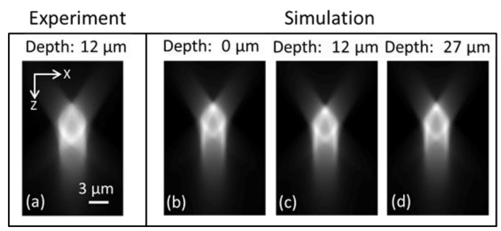

Figure 4: Comparison between experimental and simulated forward images of a 6-µm in diameter spherical shell. (a) Experimentally acquired image of a 6 µm in diameter spherical shell at depth 12 µm; Simulated image of the similar object at depths (b) 0 µm, (c) 12 µm, and (d) 27 µm. Images are shown on their own color scale to show the details. Lens: 63X/1.4 NA oil immersion objective lens, specimen embedding medium is ProLong® diamond having RI = 1.47, emission wavelength is 515 nm.

The advantage of the SQUBIC WFE system over the conventional system is experimentally demonstrated in Figure 5, where restorations from experimentally acquired images of the test object are shown. The images acquired at depths 3 µm, 12 µm, and 27 µm below the coverslip were restored using PSFs computed at 3 µm and 27 µm depths. To compute the correlation coefficients, the

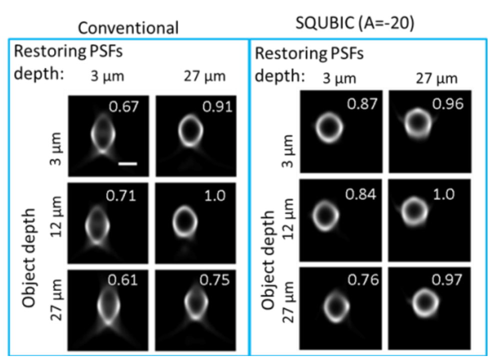

Figure 5: Performance comparison between the conventional and SQUBIC system in restoring experimental images of spherical shells at different depths. XZ sectional view of the restored images of three 6 µm in diameter spherical shells centered at depths 3 µm, 12 µm, and 27 µm in the case of conventional (left) and SQUBIC (A=-20) experimental images (right). In the experiment, as there is no true reference, the restored image that visually looks closer to a spherical shell was used as the reference for the computation of the correlation coefficients (i.e. the image at 12 µm depth restored with the PSF at 27 µm).

©2016 Society for Imaging Science and Technology
DOI: 10.2352/ISSN.2470-1173.2016.19.COIMG-157

restored image with the best spherical shape (judged by visual inspection) was considered as the reference. As evident in Figure 5, a depth mismatched PSF in the SI restoration produces significant artifacts in the case of conventional imaging compared to the SQUBIC WFE imaging. This observation is also supported by the values of the correlation coefficients (reported by the values inside each image). The standard deviations between the correlation coefficients computed for the conventional and the SQUBIC images (Figure 5) are 0.0654, and 0.0413, respectively, which indicate the reduced depth sensitivity of the SQUBIC WFE imaging system.

Summary and conclusion

In this paper, we investigated SQUBIC-WFE imaging system performance with respect to its ability to reduce the effect of depth-induced SA in wide field fluorescent microscopy. Comparisons between the SQUBIC-WFE PSFs and conventional PSFs show that, the SQUBIC WFE-PSFs vary slowly with depths compared to the PSFs of the conventional system. Simulated restored images show that in the case of SQUBIC-WFE imaging SI restoration with reduced artifacts is possible compared to conventional imaging, in which case the choice of depth of the PSF affects restoration accuracy significantly. Restored experimental images demonstrate the application of the SQUBIC WFE system in a commercial microscope and show the achieved reduced depth sensitivity of the system compared to the conventional system.

In this study, experimental implementation of the SQUBIC WFE system was limited to the design parameter $|A| = 20$ as higher values resulted in challenges of the phase mask fundamental to the SLM implementation [13] (due to the high frequency content of the phase mask at higher A). For example, experimental SQUBIC

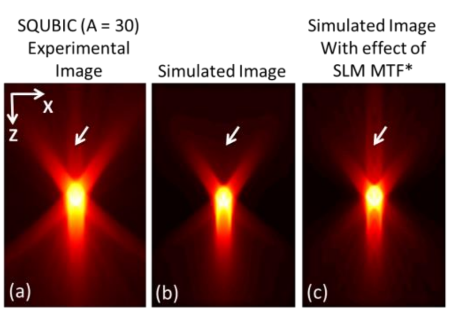

Figure 6: Forward SQUBIC WFE image comparison in the case of design parameter |A| = 30 which show the effect of SLM MTF. (a) Experimentally acquired image; (b) Simulated forward image without considering SLM MTF; (b) Forward simulated image considering the effect of SLM MTF.

WFE images are significantly different from corresponding simulated image for $|A| = 30$ (Figure 6 a & b). Although accounting for the SLM modulation transfer function (MTF) (the frequency response of the SLM) can increase the agreement between simulation and experiment [13, 18] as shown in Figure 6, it cannot describe the SLM behavior completely at high spatial frequencies. To address these challenges, in future studies, a fabricated phase mask will be used instead of the SLM to project the SQUBIC phase for higher values of the design parameter $|A|$, in order to obtain greater stability of the imaging system as predicted by the theory (Figure 2f).

ACKNOWLEDGEMENTS

This work is supported by the National Science Foundation (CAREER award DBI-0844682 and IDBR award DBI-1353904, PI: C. Preza) and the University of Memphis through a Herff Fellowship to N. Patwary. The authors are thankful to S. V. King, Research Assistant Professor at the University of Memphis, for helping with data acquisition. The authors are also thankful to Md. Shohag Hossain for measuring the MTF of the SLM.

References

[1] C. Preza, and J.-A. Conchello, "Depth-variant maximum-likelihood restoration for three-dimensional fluorescence microscopy," Journal of the Optical Society of America A-Optics Image Science and Vision, 21, 1593-1601 (2004).

[2] N. Patwary, and C. Preza, "Image restoration for three-dimensional fluorescence microscopy using an orthonormal basis for efficient representation of depth-variant point-spread functions," Biomedical Optics Express, 6(10), 3826-3841 (2015).

[3] E. R. Dowski, and W. T. Cathey, "Extended depth of field through wave-front coding," Applied Optics, 34(11), 1859-1866 (1995).

[4] S. Yuan, and C. Preza, "Point-spread function engineering to reduce the impact of spherical aberration on 3D computational fluorescence microscopy imaging," Optics Express, 19(23), 23298-23314 (2011).

[5] G. Saavedra, I. Escobar, R. Martínez-Cuenca *et al.*, "Reduction of spherical-aberration impact in microscopy by wavefront coding," Optics Express, 17(16), 13810-13818 (2009).

[6] N. Patwary, A. Doblas, S. V. King *et al.*, "Reducing depth induced spherical aberration in 3D widefield fluorescence microscopy by wavefront coding using the SQUBIC phase mask." Proc. of SPIE, vol. 8949, pp. 894911-894911-8 (2014).

[7] A. Doblas, S. V. King, N. Patwary *et al.*, "Investigation of the SQUBIC phase mask design for depth-invariant widefield microscopy point-spread function engineering," Proc. of SPIE, Three-Dimensional and Multidimensional Microscopy: Image Acquisition and Processing XXII, 8949, 894914-894914-8 (2014).

[8] N. Patwary, S. V. King, and C. Preza, "3D microscope imaging robust to restoration artifacts introduced by optically thick specimens," Proc. of SPIE, Three-Dimensional and Multidimensional Microscopy: Image Acquisition and Processing XXII, 9330, 93300O-93300O-8 (2015).

[9] J. W. Goodman, [Introduction to Fourier Optics] McGraw-Hill Book Company, New York(1968).

[10] M. Arigovindan, J. Shaevitz, J. McGowan *et al.*, "A parallel product-convolution approach for representing the depth varying point spread functions in 3D widefield microscopy based on principal component analysis," Optics express, 18(7), 6461-6476 (2010).

[11] J.-A. Conchello, and E. W. Hansen, "Enhanced 3-D Reconstruction From Confocal Scanning Microscope Images. 1: Deterministic and Maximum Likelihood Reconstructions," Applied Optics, 19(26), 3795-3804 (1990).

[12] I. J. Good, "Non-Parametric Roughness Penalty for Probability Densities," Nature Physical Sciences, 224, 29-30 (1971).

[13] S. V. King, A. Doblas, N. Patwary *et al.*, "Spatial light modulator phase mask implementation of wavefront encoded 3D computational-optical microscopy," Applied Optics, 54(29), 8587-8595 (2015).

[14] S. F. Gibson, and F. Lanni, "Experimental test of an analytical model of aberration in an oil-immersion objective lens used in three-dimensional light microscopy," Journal of the Optical Society of America A-Optics Image Science and Vision, 9, 54–66 (1992).

DOI: 10.2352/ISSN.2470-1173.2016.19.COIMG-157

[15] O. Haeberlé, "Focusing of light through a stratified medium: a practical approach for computing microscope point spread functions. Part I: Conventional microscopy," Optics communications*,* 216(1), 55-63 (2003).

[16] [Computational Imaging Research Laboratory, Computational Optical Sectioning Microscopy Open Source (COSMOS) software package; http://cirl.memphis.edu/COSMOS].

[17] Z. Wang, A. C. Bovik, H. R. Sheikh *et al.*, "Image quality assessment: from error visibility to structural similarity," EEE Transactions on Image Processing*,* 13(4), 600-612 (2004).

[18] M. S. Hossain, S. V. King, and C. Preza, "An integrated approach to determine prior information for improved wide-field imaging models from computational interference microscopy," SPIE BiOS, 933014-933014 (2015).

Author Biography

Nurmohammed Patwary is pursuing his PhD in Electrical Engineering from The University of Memphis, TN, USA. He received his BS in Electrical and Electronic Engineering from Bangladesh University of Engineering and Technology (2009), Dhaka, Bangladesh; and MS in Electrical Engineering from the University of Memphis, TN, USA (2014). His research area is computational optical sectioning microscopy.

Chrysanthe Preza is an Associate Professor in the Departments of Electrical and Computer Engineering and Biomedical Engineering at the University of Memphis since 2006, where she leads the research in the Computational Imaging Research Laboratory. She received her D.Sc. degree in Electrical Engineering from Washington University in St. Louis in 1998. Her research interests are imaging science and estimation theory with applications in computational optical sensing and imaging using multidimensional multimodal light microscopy.